

# The interplay between BMU activity linked to mechanical stress, specific surface and inhibitory theory dictate bone mass distribution: predictions from a 3D computational model

Marcelo Berli<sup>1\*</sup>, Feliciano Franco<sup>2</sup>, José Di Paolo<sup>1</sup>, Peter Zioupos<sup>3</sup> and Carlos Borau<sup>4</sup>

1-Facultad de Ingeniería, Universidad Nacional de Entre Ríos (UNER), Ruta 11, Km 10, Oro Verde, Entre Ríos, Argentina.

2-Instituto de Bioingeniería y Bioinformática, UNER, Consejo Nacional de Investigaciones Científicas y Técnicas, Ruta 11, Km 10, Oro Verde, Entre Ríos, Argentina.

3-Musculoskeletal & Medicolegal Research Group, Cranfield Forensic Institute, DA of the UK, Shrivenham, United Kingdom.

4-Multiscale in Mechanical and Biological Engineering, Department of Mechanical Engineering, University of Zaragoza, 50018 Zaragoza, Spain.

\*email: [marcelo.berli@uner.edu.ar](mailto:marcelo.berli@uner.edu.ar). Phone:+5493435183407

## Abstract

Bone mechanical and biological properties are closely linked to its internal tissue composition and mass distribution, which are in turn governed by the purposeful action of the basic multicellular units (BMUs). The orchestrated action of osteoclasts and osteoblasts, the resorbing and forming tissue cells respectively, in BMUs is responsible for tissue maintenance, repair and adaptation to changing load demands through the phenomenon known as remodelling. In this work, a computational mechano-biological model of bone remodelling based on the inhibitory theory and a new scheme of bone resorption introduced previously in a 2D model, is extended to a 3D model of the real external geometry of a femur under normal walking loads. Starting from a uniform apparent density (ratio of tissue local mass to total local volume) distribution, the BMU action can be shown to lead naturally to an internal density distribution similar to that of a real bone, provided that the initial density value is high enough to avoid unrealistic final mass deposition in zones of high energy density and excessive damage. Physiological internal density values are reached throughout the whole 3D geometry, and at the same time a 'boomerang'-like relationship between apparent and material density (ratio of tissue mass to tissue volume) emerges naturally under the proposed remodelling scheme. It is also shown here that bone-specific surface is a key parameter that determines the intensity of BMU action linked to the mechanical and biological requirements. Finally, by engaging in simulations of bone in disuse, we were able to confirm the appropriate selection of the model parameters. As an example, our results show good agreement with experimental measurements of bone mass on astronauts a fact that strengthens our belief in the insightful nature of our novel 3D computational model.

**Keywords:** Bone remodelling, finite element, BMU, bone density, specific surface.

## 1. INTRODUCTION

Mechanical properties of human bone are unique, with a tissue composition that confers the same traction strength as steel while being three times lighter [1]. This provides to the body a stiff structure for support and protection to vital organs but at the same time allowing body movement with a minimum waste of energy. Both stiffness and strength depend on the mineralization of an organic matrix which is a process that does not remain static throughout life. Bone has the remarkable ability to adapt to changing mechanical demands by two main ways: modelling and remodelling [2]. The former refers to size or shape changes with the characteristic that bone formation and bone resorption occur independently at different anatomical locations [2], [3]. Modelling occurs mainly during growth, when bone is formed without previous bone resorption or vice versa, driven by genetic factors and moderated by adaptation to prevailing loading circumstances [4]. Although globally coordinated, bone locally is

shaped or reshaped by the independent action of resorbing cells (osteoclasts) and forming cells (osteoblasts).

In contrast to modelling, in remodelling the osteoblasts and osteoclasts always work together in a coordinated way, forming the so-called basic multicellular unit (BMU) [5], [6]. Remodelling is responsible for tissue maintenance, repair and constant internal adaptation to changing loads, an endless process that continues throughout life [7]–[10]. At the same time, remodelling is the process by which homeostasis in blood calcium and other minerals is maintained by hormonal regulation through the constant mineral interchange between bone and blood [4], [11]. Both mechanical and hormonal signals are the governing factors controlling remodelling, in which after the early osteoid (organic matrix) is laid down deposition of minerals begins and creation of newly formed bone ensues [12]. Due to the dynamics of both remodelling and mineralization, each sample of bone is composed of structural units (osteons in cortical and packets in cancellous bone) that are renewed at different times, therefore presenting different levels of mineral content, leading to a heterogeneous material composition [13].

Since mass and mineral distribution are essential in the determination of the mechanical properties and biological functions of bone, the elucidation of the correct coupling between BMU activity and tissue composition in remodelling by means of a computational model is very important and it is the main objective of this work. The model is also expected to improve the numerical predictions for clinical and biological applications. This objective requires suitable implementation of the governing laws of remodelling by making assumptions related to: i) remodelling dynamics regulation, and ii) surface associated events. Both are described below.

i) First, remodelling is a spontaneous action that can be only mechanically and hormonally regulated, but not stopped. This is in line with inhibitory theory proposed by Martin [14] who proposed that remodelling is controlled but not originated by mechanical loads. The internal mechanic-sensing cells, called osteocytes, send inhibition signals through an interconnected network of channels, named canaliculi, to the bone surface (mechanotransduction). At the surface, the covering cells named lining cells start the remodelling process by sending signals to activate and recruit osteoclasts. Under Martin's hypothesis, this process is constantly being activated and the signals coming from osteocytes may only moderate the intensity of the BMU activity [3], contrary to other theories postulating that osteocytes sense mechanical stimuli and initiate remodeling to modify the bone structure accordingly (see Martin [14] and references therein). These load-linked signals control the number of BMUs activated per unit volume and per unit time [7], [10], [15] and, at the same time, regulate the net bone deposited or resorbed by each BMU depending on how the load magnitudes compare to those that under normal daily routines would maintain homeostasis [4]. Inhibitory theory states that BMUs activity rates are higher in cases of disuse and damage, which is experimentally observed [14]. For example, astronauts facing microgravity can lose significant amounts of bone mass if they do not perform adequate physical exercise [16], [17]. This means that in absence of loads, BMUs remodelling activity is very intense, leading to a net loss of bone, which is of great interest in aerospace research [17], [18].

ii) Other important considerations, related to the way BMUs operate, are the surface associated events. There are two important aspects in this respect: surface to volume ratio (specific surface area) and the osteoclasts resorption pattern. The former is a key

factor because all BMU actions always start on surfaces (such as this on the inside of Haversian channels or around the trabeculae) where remodelling signals come from [19]–[21]. The larger the available specific area, the greater the resorption activity and vice versa, as was pointed out by previous numerical studies [21]. The available surface depends of course on the level of porosity of this tissue. Martin [22] presented the parabolic curve of the specific surface of bone throughout the whole range from very compact (cortical) to least dense (cancellous) at the bottom end and showed that the maximum area available, through which remodelling acts, shows a maximum somewhere in between for porosity levels in the  $[0.3\pm 0.7]$  range (See Fig. A.1 in supplementary material). On the other hand, osteoclasts lead in the remodelling process followed by the osteoblasts. In fact, osteoclasts are responsible for bone being the only organ that contains a cell type whose only function is to constantly destroy it, and which, in healthy individuals, is counterbalanced by cells employed in bone formation [20, 24]. However, the pattern by which osteoclasts resorb bone is a key factor in determining the local mineral content of the tissue. Although it is well known that they remove bone starting from the surface, how exactly this phenomenon regulates bone mineralization is not completely understood. In this sense, computational models allow exploring the link between osteoclast resorbing dynamics and mineral content, which is very difficult to assess by in vivo observations. Several computational models dealing with remodelling and the mineralization process of bone can be found in the literature, each one of them making different assumptions. For instance, Martínez-Reina et al. [10] developed a macroscopic model assuming that osteoclasts digest bone both at the bone surface (younger) and at the core bone (older) in the same manner. This approach allowed tracking different bone variables over time (volumes, densities, mineralization) but was unable to consider geometrical effects. In this sense, Hartman et al. [25] implemented a microscopic stochastic model in which bone resorption was performed only on the bone surface but in a random process not controlled by mechanical stimuli. Such surfaces may be the outermost surface surrounding a trabecula, which is less mineralised, and may even appear in the core of a trabecula (inner surface) where the highly mineralised tissue resides. They concluded that the discrepancies between their results and some experimental data may arise from the concept that osteoclasts resorb preferentially low mineralized young bone and only at the outer bone surface. Indeed, measurements on cancellous bone made by Lukas et al. [26] confirmed that bone gets more mineralized toward the core of the trabecula, suggesting that osteoclasts action depends on the depth from the surface [27].

Taking all this into account, we proposed, in a previous work [7], a resorption scheme in which osteoclasts tend to resorb bone material closer to the surface. When testing the computational model on small samples from different internal zones of bone under equilibrium loads, the predicted relationship of apparent density  $\rho_{app}$  (mineralized wet mass over the sample volume  $V_t$ ) to material density  $\rho_{mat}$  (mass over the volume occupied by the material itself) showed an excellent agreement with experimental measurements made by Zioupos et al. [28]. However, these predictions were performed on individual bone samples under 2D loading conditions, unlinked to each other. The natural evolution of this approach is to extend and test our previous model on a 3D bone geometry under physiological loading (normal walking conditions) to investigate whether predictions on internal bone mass distribution and BMU activity are consistent with experimental observations, which is the main goal of the present work.

Therefore, a mathematical scheme of bone remodelling was computationally implemented on a 3D geometrical model of proximal human femur. Inhibitory theory and the proposed resorption strategy developed in [7] were included, which lead to interesting biological connotations of how bone is remodelled and mineral is distributed within a full 3D geometry which, as far as authors are concerned, has not been reported previously in computational studies. Our results aim to show that under the proposed hypotheses (realistic 3D geometry and normal walking loads), the model is able not only to reach a natural-like internal bone mass distribution but also internal bone densities in accordance with experimental (physiological) measurements. Also, by mathematical scheme, load-specific conditions effects, such as microgravity or sedentary situations, can be investigated.

## 2. MODEL

In this section, we summarize the mathematical model, providing greater detail for the parts which are more closely related to the present research hypothesis and to the numerical results. This section is self-contained and sufficient to understand the main equations, with a more thorough description of the model detailed in previous works [7, 10, 15] In addition, a brief description of some equations and methods used in this work is included in the supplementary material.

All the equations subsequently described, are computed for every Gauss point of the finite element mesh that represents the bone geometry (4 Gauss points per element). Each of these points will be referred to as “bone sample” henceforth.

### 2.1. Tissue composition

Due to the remodelling process both apparent density  $\rho_{app}$  and material density  $\rho_{mat}$  are regulated in response to systemic mineral demands or changing mechanical stresses. Considering only mechanical-driven changes in this work, the evolution of both densities requires the knowledge of the bone tissue composition in response to mechanical stresses.

Bone can be considered as a solid matrix material containing pores (see Fig. 1). The solid matrix is a composite of organic matrix, water and mineral content, while the pores are voids containing bone marrow, blood vessels and nerves. In this work, pores are assumed to have no mechanical influence compared to the matrix stiffness. Then, the reference volume of a bone sample ( $V_t$ ) can be divided into the volume of the tissue matrix ( $V_b$ ) and the empty volume of pores ( $V_p$ ) (see Fig. 1). In turn, the volume of tissue matrix can be divided into further sub-volumes corresponding to the mineral phase ( $V_m$ ), the organic phase ( $V_o$ ), and water ( $V_w$ ). Each sub-volume may be changing, maintaining the following relationship:

$$V_t = V_b(t) + V_p(t) = V_m(t) + V_o(t) + V_w(t) + V_p(t) \quad (1)$$

In order to describe the evolution of each sub-volume of a bone sample, the following relationships are defined:

$$v_b(t) = \frac{V_b(t)}{V_t}; \quad v_m(t) = \frac{V_m(t)}{V_b(t)}; \quad v_o = \frac{V_o(t)}{V_b(t)}; \quad v_w(t) = \frac{V_w(t)}{V_b(t)} \quad (2)$$

We consider  $v_o$  to have a constant value of 3/7 [21], and water is assumed to be replaced by mineral during the mineralization process. Hence, the next expression holds:

$$v_m(t) + v_o + v_w(t) = 1 \quad (3)$$

Once every sub-volume is determined, the density of the tissue itself (material density) can be computed as follows:

$$\rho_{mat}(t) = \rho_m v_m(t) + \rho_o v_o + \rho_w v_w(t) \quad (4)$$

where densities of mineral phase, organic phase and water are  $\rho_m = 3.2 \text{ g/cm}^3$ ,  $\rho_o = 1.1 \text{ g/cm}^3$  and  $\rho_w = 1.0 \text{ g/cm}^3$ , respectively [10].

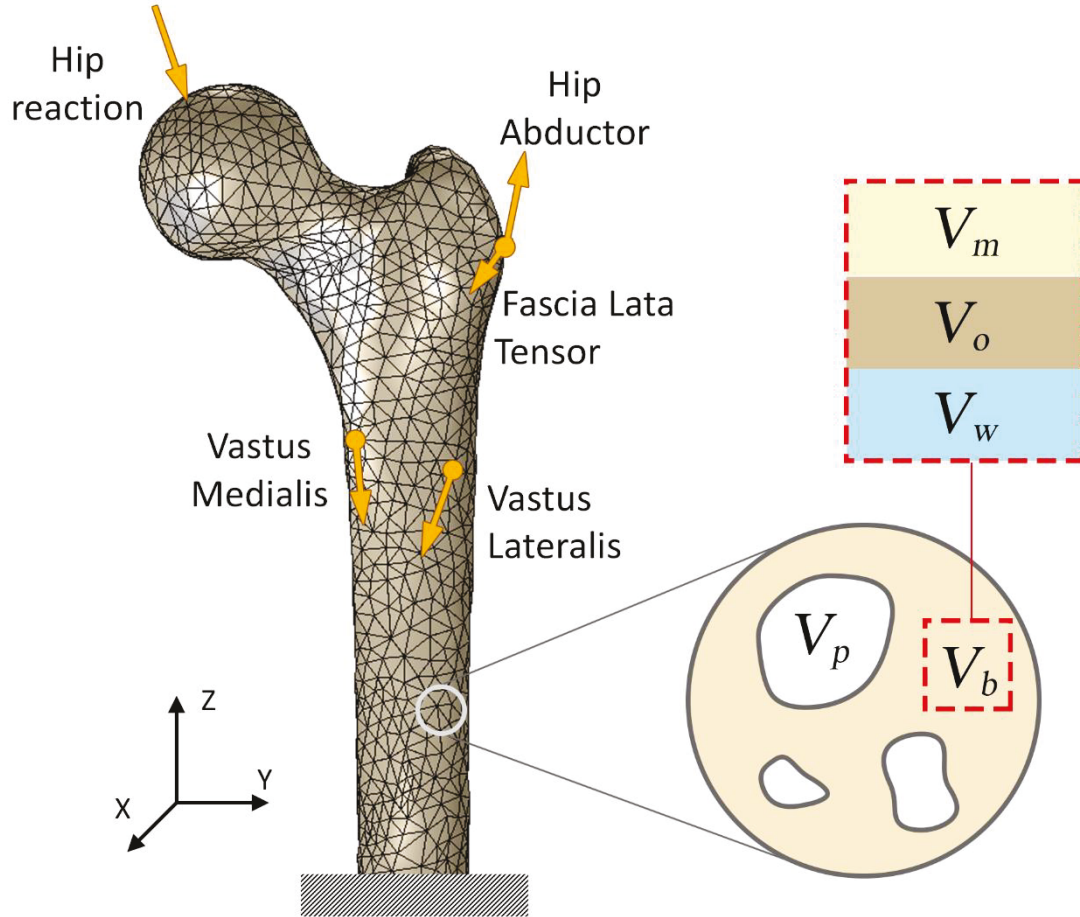


**Figure 1.** Volume of a bone sample, where  $V_b$  is the volume of tissue bone matrix and  $V_p$  the volume of pores. Bone matrix consisting of: organic matrix, water and mineral content so that  $V_b$  can in turn be divided into further sub-volumes corresponding to the mineral phase ( $V_m$ ), the organic phase ( $V_o$ ), and water ( $V_w$ ).

Note that in equation (4), the organic phase does not change over time. Hence, material density only changes due to the replacement of water by mineral phase. On the other hand, apparent density is the main variable in most of the remodelling models, which is related to material density as follows:

$$\rho_{app}(t) = \rho_{mat}(t)v_b(t) \quad (5)$$

This density can change by both mineralization (changes of  $\rho_{mat}$ ) or tissue volume variation due to the remodelling process. Material density is more closely linked to mineral content, while apparent density indicates a more general composition of the tissue.

Another variable that can be used to track the mineral content is the ratio of mineral mass and dry tissue mass:

$$\alpha = \frac{\rho_m v_m}{\rho_m v_m + \rho_o v_o} \quad (6)$$

## 2.2. Remodelling dynamics.

Bone tissue responds to changing mechanical demands and/or systemic mineral requirements by moderating the remodelling process [7]. Through this process, some pieces of bone are formed ( $v_f$ ) while others are removed or resorbed ( $v_r$ ) at any given point in time, thus updating each bone volume fraction ( $v_b$ ). Therefore, the net rate of change of the volume fraction ( $\dot{v}_b$ ) depends on the difference between removal and deposition rates:

$$\dot{v}_b(t) = \dot{v}_f(t) - \dot{v}_r(t) \quad (7)$$

Computation of each term on the right-hand side of equation (7) can be found in a recent paper of ours [7]. Both bone formation and resorption rates are driven by the number of BMUs activated per volume unit and time unit  $\dot{N}_{UBM}$  by the following relationship:

$$\dot{N}_{UBM} = \frac{\partial N_{UBM}}{\partial t} \left[ \frac{N_{UBM}}{mm^3 dia} \right] = f_{act} S_v \quad (8)$$

where  $S_v$  is the specific surface and  $f_{act}$  the activation frequency.  $S_v$  is modelled by considering the inhibitory theory [22], which stipulates that those areas with very high or very low porosities (low  $S_v$  values) will have a low influence on the activation rates (and hence on BMUs activity), while in areas with intermediate porosity values this influence is significantly greater, as was pointed out by Pivonka et al. [21].

Based on previous works [30], the activation frequency  $f_{act}$  is proposed as follows:

$$f_{act} = f_{bio} (1-s) \quad (9)$$

where  $f_{bio}$  is a biological factor accounting for hormonal and metabolic influences, and  $s$  is the normalized level of the inhibitory (mechanical) signal, which can take values between 0 and 1. In this work, it will be assumed that the metabolic factor remains constant (see table 1), while the inhibitory signal comes from the mechanical stimulus sensed by the osteocytes network. Any variation in the reception of this signal can cause different levels of activation. For instance, the two extremes at which the signal is cancelled are disuse, in which mechanical stimulus is zero, and damage, for which the signal transmitted from the osteocytes to the lining cells is interrupted. These extremes are associated with zero load or overload, respectively, while intermediate levels of mechanical stimulation involve signals that reduce the UBM activation cascade to varying extents. In this model, the hypothesis of previous works is maintained in that

this inhibitory signal depends on the mechanical stimulus  $\xi$  and the level of damage  $d$ . This dependence is proposed as follows:

$$s(\xi, d) = \frac{\xi}{\xi + c} (1 - d)^a \quad (10)$$

where  $c$  and  $a$  are parameters weighting the level of transduction associated with these purely mechanical variables (see table 1). The damage  $d$  is a normalized variable indicating the level of tissue damage. A value of  $d = 0$  implies an undamaged tissue while a value of  $d = 1$  is indicative of a totally damaged tissue with no local load-bearing capacity [30]. Computation of this parameter is composed of both the assessment of fatigue damage through the degradation of the elastic modulus extracted from experimental tests performed by Pattin et al. [31] and the daily repair due to the remodelling process [10] (see more details in the paper by García Aznar et al. [30]). On the other hand, the mechanical stimulus  $\xi$  is defined in terms of a scalar quantity following Mikic and Carter [32], which represents the daily strain history and, therefore, depends on the strain level and the number of cycles ( $N$ ) for each load case  $i$  as follows:

$$\xi = \left( \sum_i N_i \bar{\varepsilon}_i^m \right)^{\frac{1}{m}} \quad (11)$$

where  $m$  is an empirical exponent that weights the relative importance of the strain level and the number of cycles in the mechanical stimulus. Typically, a value of  $m=4$  is adopted [30], [32]. The strain level is computed through the stress functional defined as:

$$\bar{\varepsilon} = \sqrt{\frac{2U}{E}} \quad (12)$$

where  $U$  is the strain energy density [30] and  $E$  the isotropic elastic modulus defined as follows [10], [30]:

$$E = 84370 v_b^{2.58} \alpha^{2.74} (1 - d) [MPa] \quad (13)$$

The net bone deposited or resorbed depends on the focal balance [7], which follows a piece-wise linear model as a function of the unbalanced stimulus  $\xi - \xi^*$ ,  $\xi^*$  being the reference (daily normal) stimulus [30]. If  $\xi = \xi^*$ ,  $\dot{v}_f(t) = \dot{v}_r(t)$  and  $\dot{v}_b(t) = 0$  (equilibrium). For higher stimulus,  $\xi > \xi^*$ , bone formation dominates ( $\dot{v}_b(t) > 0$ , porosity decreases), while for disuse,  $\xi < \xi^*$ , resorption dominates ( $\dot{v}_b(t) < 0$ , porosity increases). It should be noted that the equilibrium stimulus can adapt to a sustained stimulus by means of an exponential law of adaptation as can be seen in the supplementary material and in the work of García-Aznar et al. [30]. Finally, the cross section of the material volume unit resorbed by osteoclasts and then filled by osteoblasts is taken into account. Osteon cross section is considered for the assumed range of cortical bone ( $v_b > 0.7$ ), while hemi-osteon is considered for cancellous bone ( $v_b < 0.3$ ) [20]. In the transition zone, where  $0.3 < v_b < 0.7$ , a linear transition approach of the BMU section is assumed. (More details in supplementary materials and references [7], [30].)

### 2.3. Mineralization and resorption strategy

Mineralization process involves three phases: i) resting time, during which no mineral deposition takes place, ii) primary phase with a linear increase of mineral, and iii) secondary phase with an exponential growth of mineral content. These phases are modelled as follows [10]:

$$v_m^*(t) = \begin{cases} 0 & \text{if } t \leq t_{nm}; (\text{Fase i}) \\ \text{ii): } v_m^{prim} \frac{t - t_{nm}}{t_{prim}} & \text{if } t_{nm} < t \leq (t_{nm} + t_{prim}); (\text{Fase ii}) \\ \text{iii): } v_m^{max} - (v_m^{max} - v_m^{prim}) e^{-\kappa_m(t - t_{prim} - t_{nm})} & \text{if } (t_{nm} + t_{prim}) > t; (\text{Fase iii}) \end{cases} \quad (14)$$

where  $t_{nm}$  and  $t_{prim}$  are the resting and primary phase times respectively and  $\kappa_m$  is a parameter that measures the rate of mineral deposition in the secondary phase.  $v_m^{prim}$  is the specific volume at the end of the primary phase ( $v_m^{prim} = 0.121$ ) and  $v_m^{max}$  corresponds to the specific volume for the maximum possible calcium content ( $v_m^{max} = 0.442$ , 300 mg/g) [33]. To calculate the mineral volume ( $v_m$ ), a mineralization law is established. Volume fraction  $v_b$  is composed of material remnants created on the day  $\tau$  previously and still present at the current time  $t$ :

$$v_b(t) = \int_{t - T_m^{Max}}^t \frac{dv_b(\tau)}{d\tau} d\tau \quad (15)$$

where  $T_m^{Max}$  is the time required for a piece of bone to reach maximum mineral content. With each time increment the volume fraction is, it must be updated by considering the amount of bone formed ( $dv_f(t) = \dot{v}_f(t)dt$ ) and resorbed ( $dv_r(t) = \dot{v}_r(t)dt$ ). We assume that osteoclasts tend to remove bone mainly from those structural units that are younger and closer to the surface and at the same time those that have already passed the resting phase, as discussed in our previous work [7]. Because this model is continuous and surface structural units cannot be spatially identified, the selection of the pieces that meet the above requirements is done by accounting the time since they were created. That is to say, every bone sample is actually divided into 4000 bone pieces created at different times and therefore having different mineralization levels. A time window ( $\Delta\tau = t_{sr}$ ) is defined for the purpose of resorption candidate selection. If the lower limit of this window is denoted as  $t_{nm}$  (end of the resting phase), then the bone pieces to be digested in each activated BMU (bone sample) are those in the interval between  $t_{nm}$  and  $t_{nm} + t_{sr}$  days ago. Thus, the mineral volume  $v_m(t)$  can be computed as:

$$\begin{aligned} v_m(t) &= \frac{1}{v_b(t)} \int_{t - T_m^{Max}}^t v_m^*(t - \tau) \frac{dv_b(\tau)}{d\tau} d\tau = \\ &= \frac{1}{v_b(t)} \int_{t - T_m^{Max}}^t v_m^*(t - \tau) \frac{dv_f(\tau)}{d\tau} d\tau - \frac{1}{v_b(t)} \int_{t - t_{nm} - t_{sr}}^{t - t_{nm}} v_m^*(t - \tau) \frac{dv_r(\tau)}{d\tau} d\tau \end{aligned} \quad (16)$$

where  $v_m^*(t - \tau)$  is the mineral volume fraction of each piece of bone, calculated according to equations (14). We assume that the resorption window size varies proportionally to

the available bone material specific surface:  $t_{sr} = k_{sr}S_v$ , where  $k_{sr}$  is a scaling parameter to control the window resorption size (see supplementary materials or [7]).

#### 2.4. Mechanical model.

The remodelling process is implemented inside a 3D model of the proximal part of a human femur. Figure 1 shows the applied loads and constraints on the 3D geometrical model and table 1 their values, according to Martínez Reina et al. [34], who in turn extracted them from Heller et al. [35]. The loads correspond to those at 25% of the gait cycle. This is the instant of maximum loading of the femur during normal walking and provides the amplitude of strain energy density to evaluate the mechanical stimulus [34] by considering  $N= 10.000$  daily cycles (steps, see equation 11). All forces on the modelled bone are therefore a consequence of body weight and accelerations during normal walking. Not only hip contact transmits forces but also all muscles from adjacent bones. As was considered by Martínez-Reina et al. [34], loads simulate the reactions at the hip joint and the muscle forces applied in the femur during walking. Only those muscles that are predominant during the gait cycle have been considered, i.e. hip abductors, tensor fasciae latae, vastus lateralis and vastus medialis. Martínez-Reina et al. [34] extracted this from Behrens et al. [36] and we followed their approach to simulate the most exigent condition under walking. It is worth noting that simulations with climbing stair load conditions were also performed, but no significant differences were found as compared to the normal walking. These preliminary results can be consulted in Supplementary Materials

Bone is assumed as an isotropic inhomogeneous linear elastic solid. Following García-Aznar et al. [30], we have assumed that the Poisson ratio is set to a constant value of 0.3. The base of the geometrical model is completely constrained, i.e. zero displacements and rotations.

Force	Fx [N]	Fy [N]	Fz [N]
Hip reaction	-451.4	225.7	-1806
Hip abductors	468	0	694
Tensor fasciae latae	-117	158.8	-75.2
Vastus Medialis	-8.4	-33.4	-167
Vastus Lateralis	-8.4	-108	-543

**Table 1:** Applied loads during walking on geometry of figure 3, extracted from Martínez-Reina et al. [34] and Heller et al. [35].

### 3. METHODS

The mechanical model was implemented in Abaqus 6.14 (Finite Element software), while the computational algorithm for the remodelling process was implemented in FORTRAN language in a User Material subroutine (UMAT), which is linked to the Finite Element solution of the mechanical problem at each iteration. While the loads are statically imposed, their cyclic application impacting on bone remodelling is considered by evaluating the mechanical stimulus of a cyclic load through equation (11). This simplifies the resolution procedure because it is possible to model an inherently non-stationary but slow process by imposing representative static loads.

Figure 2 illustrates in more detail the procedure of the computational method. Each

simulation cycle involves one day of evolution. In some cases, 22 years are needed to reach steady state (using the criterion proposed by Martínez-Reina et al. [34]), for which approximately 8000 iterations are needed. To reduce the simulation time, a mesh with 13500 quadratic tetrahedral elements (10 nodes each) was obtained by means of a convergence study (See supplementary materials). Densities at every point are computed in a post-process stage since the state variables of the bone tissue are bone volume fraction ( $v_b$ ) and mineral volume ( $v_m$ ), while organic volume fraction remains constant after osteoid is created and water is replaced by minerals. Finally, material and apparent densities are computed via equations (4) and (5) respectively.

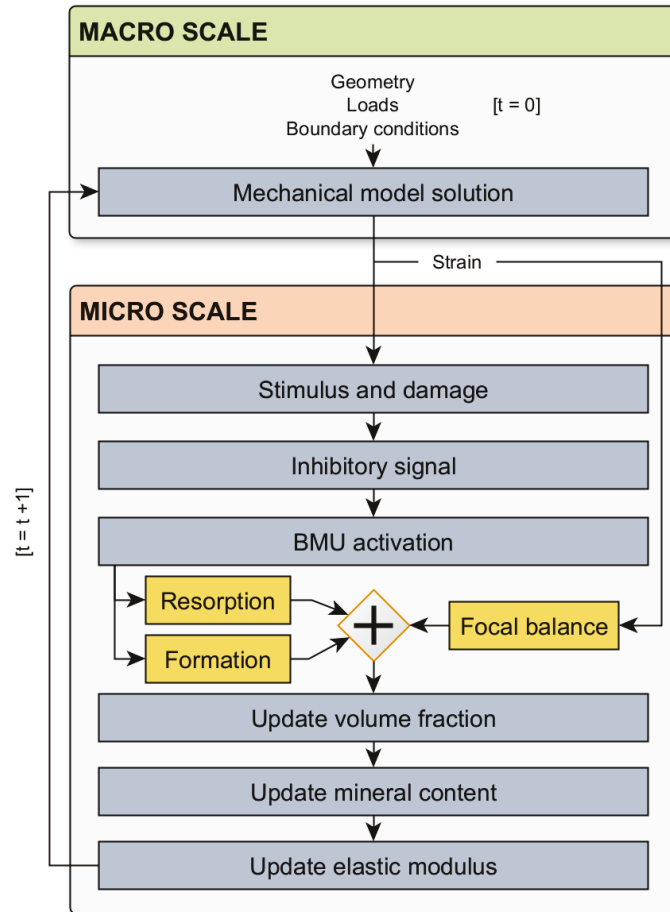


**Figure 2:** Iterative scheme of the numerical algorithm to solve the coupled remodelling-mechanical problem. The process starts by proposing the initial value of the parameters. Using the Abaqus software, the mechanical problem is solved by obtaining the deformation field by means of the finite element method. Then remodelling process is solved in a UMAT and the value of the elastic parameters of the material is updated by means of an algorithm implemented in Fortran language. The process continues until steady state is reached, for which a convergence criterion is evaluated.

Parameter		Value
$m$	Weighting exponent	4
$a$	Damage activation exponent	40
$c$	Reference equilibrium stimulus	0.025
$f_{bio}$	Biological frequency factor	0.005

$\xi^*$	Initial reference stimulus	0.00075
$\kappa_{sr}$	Scaling parameter controlling the size of the resorption window	170 days *
$\kappa_m$	Rate of secondary phase	0.0005
$T_{nm}$	Mineralization lag time	12 days
$T_{prim}$	Length of primary phase	10 days
$T_m^{max}$	Time to reach the maximum mineral level	4000 days

*Table 2: Parameters values of the model. Values of the scaling parameter between 50 and 3000 days were also used, but the optimum that allows fitting the numerical results to the experimental measurements is the one reported in the table.*

## 4. RESULTS AND DISCUSSION.

### 4.1 Bone apparent density distribution depends ultimately on external loads in normal circumstances.

To understand how the final density distribution depends on the starting conditions, we performed simulations with different homogeneous initial density distributions. i.e. different initial mass, and let them achieve a steady state. The aim was to address the following hypothesis: given a real external bone shape and a load system under normal walking, can the BMUs activity lead to a final natural and optimal bone density distribution that meets both the biological and mechanical requirements?

The initial apparent densities were selected by considering four different initial bone volumes (0.3, 0.5, 0.7 and 0.94) to cover porosities from cancellous to cortical bone. All cases started with initial uniform density distribution, i.e. identical bone volume and mineralization for all the internal points of the 3D domain. Figure 3 shows that the final total mass values computed for all cases were very close to each other (6% maximum difference). It is worth mentioning that the steady state density distribution was not expected to be unique for this mechano-biological model because there are variables linked to BMUs activity like equilibrium stimulus, stimulus accommodation and damage that depend in turn on initialization conditions. For example, equilibrium stimulus and damage both play a disrupting role when initialization conditions are not consistent with the applied loads, as can be seen for  $v_b^0 = 0.3$  (see Fig. 3). For a very low value of  $v_b^0$  (high porosity) and real loads, high stresses are expected over the whole bone volume, leading to a fictitious deposition of tissue in areas where high porosity would be expected in a real bone. At the same time, damage rises notably (see Fig. 4) leading to high remodelling rates throughout the entire tissue and therefore preventing the development of higher densities at the cortical areas that do not have enough time to settle their mineral content. In fact, for the case of  $v_b^0 = 0.3$ , the steady state apparent density distribution (see Fig. 3) is quite different compared to that of a natural case, with large damaged areas and very high rates of BMU activity (see Fig. 4).

On the other hand, when loads are appropriate to the initial bone state (or vice versa), the model is able to reach a density distribution similar to that of a real bone as shown

in figure 3. For example, for  $v_b^0 = 0.94$ , very low damage values and BMU activity are registered only at few specific zones (see Fig. 4) where biological requirements should be met, as will be discussed later. This means that a load supporting configuration different to that of a natural one is possible for the remodelling process, but with a higher energy cost and constant risk to develop high damage and fracture. For  $v_b^0 > 0.5$  and real loads, the model can reach a mass distribution similar to a real bone. All in all, the final bone apparent density depends ultimately on external loads, with little effect of the initial conditions provided these are able to sustain the initial damage if the load/initial state relationship is too asymmetric.

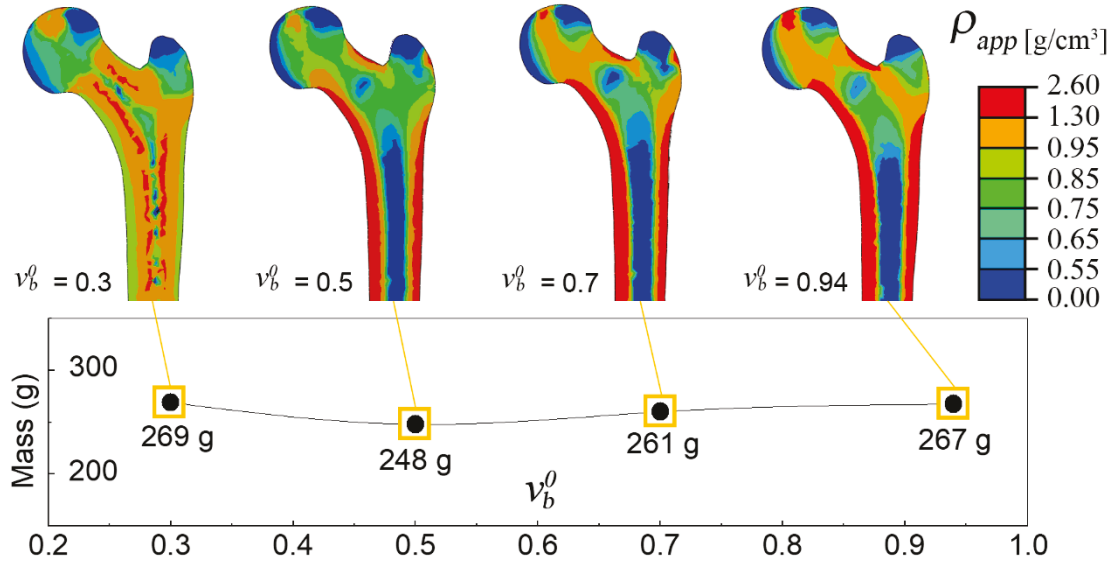


**Figure 3.** Top: Final density distribution for the four bone volume homogeneous initializations ( $v_b^0$ ). Note that for the cases of  $v_b^0 > 0.5$ , the mass distribution is similar to that of a real bone. Bottom: Total mass computed for the converged situation. Maximum difference of 6% is found between  $v_b^0 = 0.5$  and  $v_b^0 = 0.94$ .

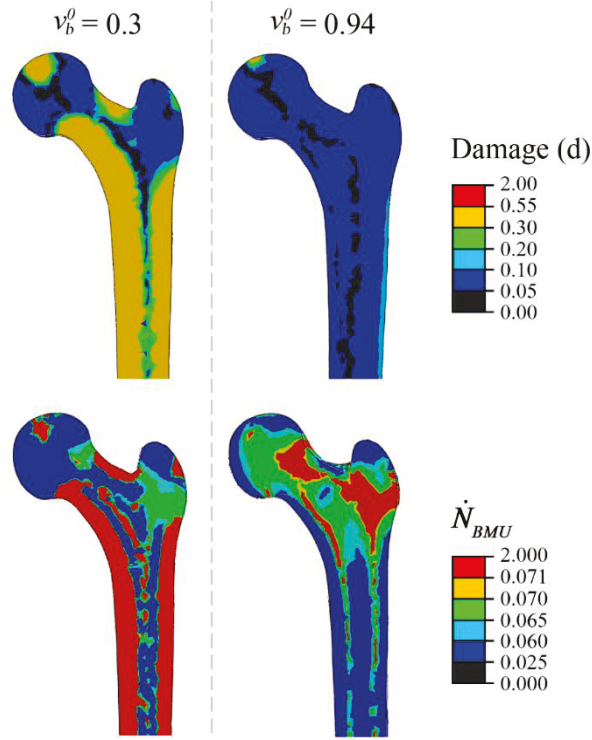


**Figure 4.** Top: Damage of converged simulations for two initializations:  $v_b^0 = 0.3$  (presenting high damage values) and  $v_b^0 = 0.94$  (with low damage values). Both situations correspond to those of Fig. 3 for the corresponding  $v_b^0$  values. Despite both initializations reaching a final steady state in equilibrium with the applied loads, the situation for  $v_b^0 = 0.3$  is dominated by damage instead of the mechanical stimulus leading to high BMU activation rates. Bottom: Activation rate of BMUs. Note that for  $v_b^0 = 0.3$ , there are overall higher activation rates than those observed for  $v_b^0 = 0.94$ , and at zones where compact bone should develop in the natural case and higher activities would not be expected.

We will now analyze the results for a well initially-conditioned case, i.e. for  $v_b^0 = 0.94$ . It should be clarified that due to point application of loads (see Fig. 1), there will be obvious differences in localized areas between the real bone and the computational results. For example, figure 5-B shows the appearance of high apparent densities at the reaction forces area on the femoral head, where load is actually distributed over a larger area. Nevertheless, the computed results in terms of the distribution of apparent densities over the femur, have a notable similarity to those of a real bone frontal cut (Fig. 5-A), with the areas of greater (compact) or lesser (cancellous) bone mass easily distinguishable. Importantly, the computed final mass of the analyzed bone portion (267 g) is consistent with the weight measurements reported by Singh and Singh [37]. Considering the weight measurements of male bones, the computationally-predicted mass is about 70 % of the mean value reported by these authors. By taking into account that the computational geometry volume is  $276 \text{ cm}^3$ , approximately 81 % of the maximum volume of a male femur according to Maden-Wilkinson et al. [38], it can be inferred that the numerical value is within the range of measurements made by Singh and Singh [37]. This quantitative agreement suggests the plausibility of the implemented hypotheses and an adequate selection of model parameters for this initialization.

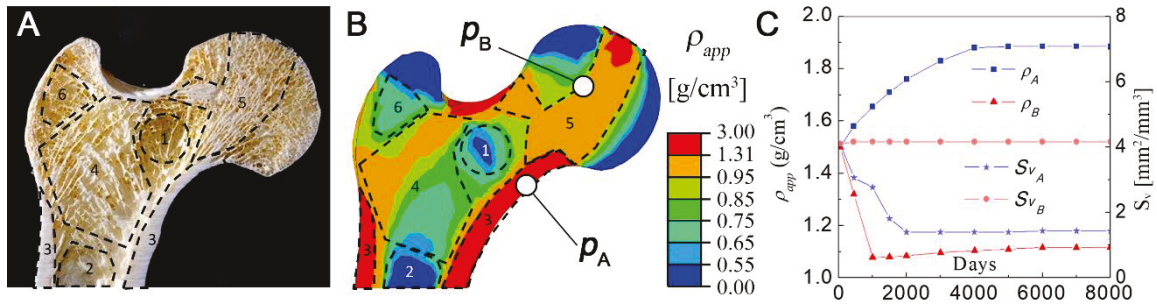


**Figure 5.** Qualitative comparison between the frontal section of the proximal zone of a human femur (A) and the result of the distribution of apparent densities of the numerical model (B). A good similarity in the marked zones is observed with respect to the distribution of the bone mass. Zone 1, called Ward's triangle, shows a reduction of bone in an area of very low mechanical stress. Zone 2: beginning of the medullary channel, containing very low apparent density. Zone 3: areas of cortical bone, with high apparent density, and a very similar morphology between both images. Zone 4: area of lower mechanical stress with variable bone densities. Zone 5: Transition zone with densities somewhat higher than the surrounding cancellous bone, which transmits the head load to the lower cortical zone. Zone 6: zone away from the loads applied to the model, with very low densities. The frontal section of the real bone was extracted from a Yale University database [39], used as a model to describe the tissue structure, which was selected for having an external morphology similar to the geometric model used in this work. C) Apparent densities of points A (blue squares) and B (red triangles) from figure 5-B.

#### 4.2 A boomerang-like shape relationship between apparent and material densities emerges naturally for different regions of the bone when applying the correct resorption strategy.

In our previous paper [7], we showed that a boomerang like relationship between  $\rho_{app}$  and  $\rho_{mat}$  emerges when testing individual bone samples under 2D loading conditions, and how the resorption strategy determines not only the very shape of experimental measurements trend but also the location of the numerical results into the experimental zone. Here we perform the same computational experiment to a 3D geometry in which every internal tissue sample is linked to each other in a computational mesh. Examining the internal structure is therefore necessary to determine whether the whole bone model acquires physiological values of densities that can be fitted to experimental data [28]. For this purpose, the material and apparent density values of twenty evenly distributed points were extracted to cover different internal parts of the bone at the proximal epiphysis, and a part of the diaphysis (see Fig. 6 A). These results are compared to experimental data from Zioupos et al. [28]. Three resorption windows were selected to investigate the effect of the resorption strategy on the mineral distribution. The first considers that only those newly created bone pieces without mineral content can be removed by osteoclasts ( $k_{sf}=50$  days). The second strategy allows osteoclasts to remove pieces at any location, from the bone surface to the core, thus attacking internal pieces with higher mineral content ( $k_{sf}=3000$  days). Finally, the strategy found optimal and

used to get the results in this work was the one considering that those superficial pieces with a minimum mineral content are preferentially removed by osteoclasts ( $k_{sr}=170$  days). All results are condensed in figure 6, including experimental measurements by Zioupos et al. [28]. It can be observed that the boomerang-like shape emerges naturally regardless the selected resorption window, since this feature is related to the link between BMU activation frequency and the free surface ( $S_v$ ), which is in turn dependent on the porosity [see supplementary materials]. However, those relations alone are not sufficient to obtain a correct qualitative and quantitative fit of the experimental measurements, but require an additional removal strategy that ultimately determines the distribution of the mineral in the bone tissue, as was showed in our previous work [7]. The strategy proposed in this work (for  $k_{sr}=170$  days) leads to a notable good fit of the experimental physiological values, confirming that the resorption dynamics is determinant for bone mineral distribution. As in the 2D case [7], it should be noted that bone with both extremes of apparent densities, i.e., the highest belonging to compact bone ( $v_b^0 > 0.7$ ), as well as the lower ones corresponding to very spongy bone ( $v_b^0 < 0.3$ ), have a tendency to acquire similar mineral contents (the highest values of material densities). For those zones with transitional densities between the two previous ones, lower mineral content and therefore lower material density values can be observed. In the next section, the possible biological and mechanical reasons for the boomerang-shape are discussed.

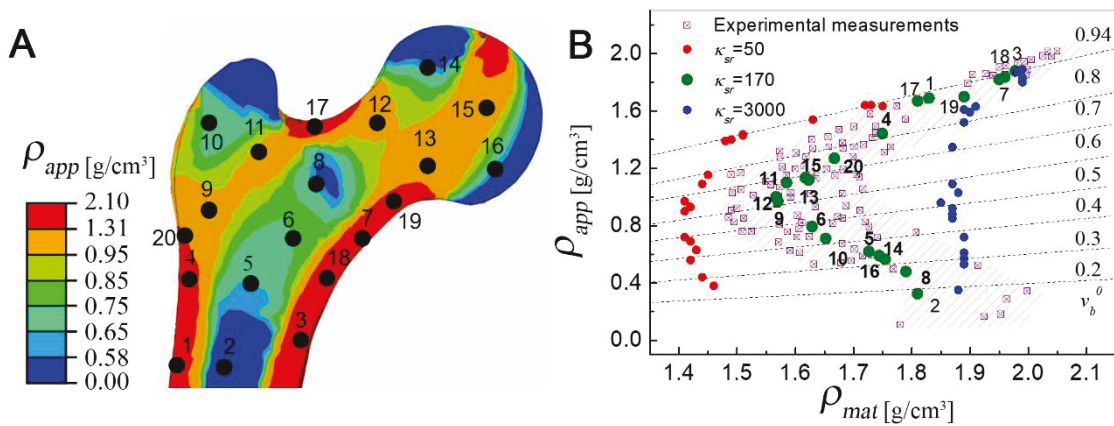


**Figure 6.** A: Proximal part of a frontal section of the femur, showing the distribution of apparent densities and the points at which the values of these densities and material densities are evaluated. B: Location of the densities predicted by the model on the experimental curve performed by Zioupos et al. [28] for three resorption windows. Note that the points for the proposed strategy (those superficial pieces with a minimum mineral content are preferentially removed by osteoclasts,  $k_{sr}=170$  days) are located within the experimental data zone, showing a good agreement between the numerical predictions and the experimental values at all points explored.

#### 4.3 Evolution of bone density is governed by mechanical and biological requirements.

The evolution of the distribution of the bone mass can be traced through the apparent density as can be seen in figure 7, which shows the different states of the bone as BMU action molds the internal structure of the tissue starting from a uniform density distribution for  $v_b^0 = 0.94$ . Every point in the bone starts with the same initial conditions.

For all simulations it is assumed that the external shape of the bone remains unchanged. If we accept this, remodelling is the physiological process by which mass and mineral content are distributed internally due to BMU action depending on both bone external shape and loads. It can be noted that the final density distribution is closely linked to mechanical demands, as has been discussed in previous sections. Although this is not the first work showing this characteristic, it does highlight the well-known fact that the action of the BMU complex is closely linked to mechanical requirements and leads to an internal structure linked to stresses. Simultaneously, figure 7 shows more clearly how the predicted BMU action is driven. Those zones with high BMU activity resulted in reduced mineral content. As the remodelling process reaches the final mass distribution, the material density increases in the less active zones (cortical and very spongy), while at the transition zones, where BMU activity is higher, material density acquired lower values. In these regions, there is an increased BMU activity due to the presence of a higher specific surface area. Consequently, an increased bone turnover results overall in the presence of younger tissue age with lower mineral content. This dynamic process may have a biological reason because the intermediate porosity zones do not receive very high loads and, at the same time, they are probably the sites where a more active exchange of calcium takes place to satisfy the systemic demands of this mineral. Indeed, it is the location of the very active red bone marrow. On the other hand, the areas with very high and very low porosity have lower specific surface values and therefore BMU activity, and as a result higher values of mineral content according to the mechanism we propose here.

For compact bone, we propose that low bone removal rate is linked to mechanical loading too. In the diaphysis, for instance, the tissue supports the highest mechanical stresses, for this reason it would not be desirable to have a high rate of turnover which would result in tissue of low mineral content. On the other hand, in the medullary channel where bone density is at its lowest, bone hosts yellow bone marrow, a tissue potentially hematopoietic of energy reserve, which has very little activity under normal conditions and a low mineral interchange with blood. For these reasons, it seems reasonable to infer that both zones (the cortical and the lowest density cancellous) have low bone removal rates, which is manifested by the rate of activation of the UBM complex plotted in figure 7 for the converged situation ( $t=8000$  days). These arguments provide an initial insight into why the dynamics of bone remodelling is so closely linked to its level of porosity to match at the same time both biological and mechanical demands under normal conditions and leading to both apparent and material density distribution that efficiently supports the loads.

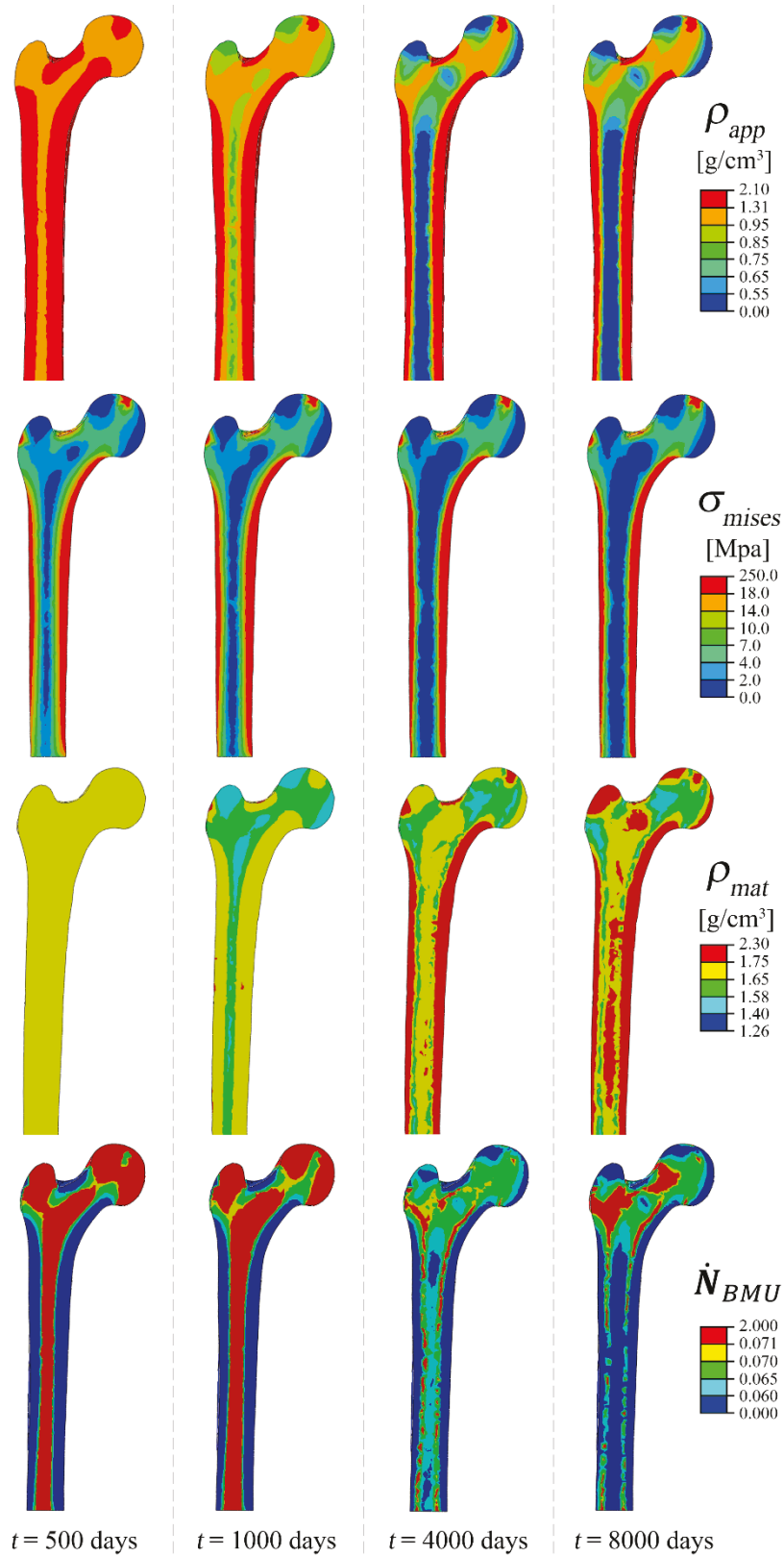


**Figure 7.** Evolution images for  $v_b^0 = 0.94$ . From top to bottom: First line: Evolution of the distribution of apparent densities in a frontal section of the femur, starting from a uniform distribution of  $1.5 \text{ g/cm}^3$  at  $t=0$  days. Second line: von Mises stress. The relationship between mechanical stresses and apparent densities is remarkable. Note that apparent density is higher at those places where stresses are higher too, showing a link between the mass distribution and the mechanical requirements. The apparent

density value of  $1.3 \text{ g/cm}^3$  considered as a natural separation from compact to cancellous bone was proposed by Zioupos et al. [28]. Third line: Material density. Note that mineral content tends to increase in areas of cortical and very spongy bone, which is manifested by high material density values. Fourth line: BMU activation rate ( $\dot{N}_{UBM}$ ). Note that the highest values of  $\dot{N}_{UBM}$  (higher BMU activity) for the converged situation (8000 days) appear in areas of lower mineral content. During the first stages, it can be noted that higher activity is manifested in those areas where mass rapidly decreases.

---

#### **4.4 The specific surface plays a dominant role in the remodelling scheme.**

As pointed out in the previous section, the connection between BMU action and specific surface plays an important role in the remodelling process. For instance, points A and B in figure 5-C are in areas of growing and decreasing density respectively. Initially, differences in mechanical stimulus drive the net deposition or resorption, being density decrease at point B much faster than the increase at point A. The starting value of porosity for both points is 0.3, while the final values are 0.08 for point A and 0.55 for point B. Hence,  $S_v$  value of point A decreases (see Fig. 5-C) leading to a lower BMU activity. Conversely,  $S_v$  value for point B is maintained at high values along the complete simulation period, and therefore undergoing to higher BMU activities. At the same time, the implemented stimulus model according to inhibitory theory enhances this effect since a lower mechanical stimulus for point B reduces the inhibitory signal and increases the activation rate of the BMUs. The final densities of both points are equidistant above and below the initial density, but density of point B reaches the final value at day 1000 while point A does at day 4000. In other words, it takes four times as long to reach a higher density than the time required to lose the same amount of density. It is important to note that due to the combination of the inhibitory theory and surface effects, the apparently “unnecessary” mass, i.e. the tissue for which initial equilibrium stimulus is above the actual mechanical stimulus (point B), is rapidly lost, while the required increase of mass to mechanically reinforce the bone (point A) occurs much more slowly. Conceptually, these results are consistent with experimental data from space travel experiences. In particular, Grimm et al. [17] state that following spaceflight, the time required for astronauts to recover lost bone mass exceeds the length of the mission by a factor of three to four times. The possible reason for this behaviour could be evolutive, i.e., it could be vital for the structural tissue to be as light as possible to reduce the movement effort in order to assure survival. At the same time concentrating the strong tissue parts in minimum areas could be the driving concept which defines the internal distribution of mass in the bone. Or may be that it is essential to assure a constant supply of minerals to maintain vital organs functioning while absence of loads does not allow to generate bone at the same rate it is being resorbed. These are subjects of future works.

#### **4.5 Absence of external loads leads to severe bone mass loss and redistributes the apparent densities.**

To test whether the model parameters (adjusted to achieve density distributions similar to that of real ones) were well suited for other kind of conditions, we removed the external loads and performed simulations of a “disuse” state. For that, we used the

converged bone obtained from our previous simulations as initial state (density distribution under loads of table 1, situation corresponding to figure 5-h). A disuse period of two years was chosen to investigate the possible effect of unload bones during long periods. As figure 8 (middle) shows, there is a larger decrease in the first year and then the decrease is almost linear until the end of the second year. At the end of the simulation period, the total bone mass is about 60 % compare to the initial mass.

Figure 8 also shows the loss of bone mass in all areas of the tissue after one year of disuse. It should be noted that the cortical area on the right side of the diaphysis experiences a decrease in densities below  $1.3 \text{ g/cm}^3$ , i.e., it becomes a transition bone (from cortical to cancellous bone) according to the suggested separation of Zioupos et al. [28]. When mechanical loads are removed, the bone balance favours resorption and, as the bone volume is reduced mainly in high densities zones, porosity increases and an accelerated process of bone loss is generated due to the link to specific surface, which is further increased by the totally absence of an inhibitory signal. The result is a reduction in bone mass from 267g (normal bone) to 203g (after 350 days, almost one year of disuse), thus computing a decrease of approximately 23.9 % (see Fig. 13). According to the work published by Grimm et al. [17], an astronaut can lose up to 2% per month of bone mass in the absence of gravity. Hence, the reduction predicted by the present model for almost one year of disuse is in agreement with the observations of Grimm et al. [17]. This means that when the model starts with a real initial density distribution, it is able to mimic the evolution of bone mass in microgravity conditions at least for one year.

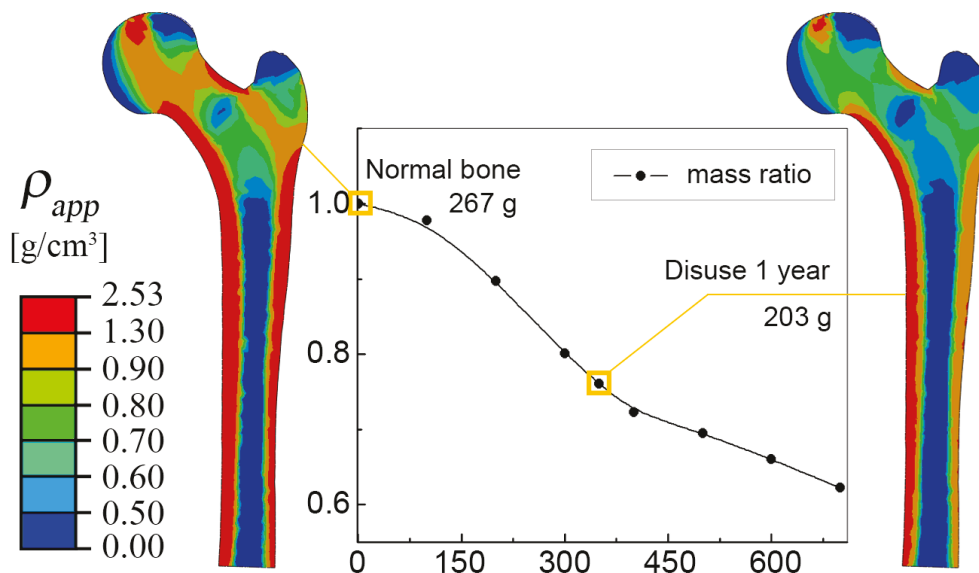


**Figure 8:** Distribution of apparent densities for a bone under the loads in Table 1 before (left) and after (right) one year of disuse. In the middle the graph shows the loss of bone mass during two years of disuse. The mass is normalized to the initial mass at the start of the disuse period.

## 5. CONCLUSIONS

A 3D computational model of bone remodelling was implemented to show how a dynamic remodelling process, in which BMU action linked to surface characteristics under Martin's inhibitory theory drives the evolution of internal apparent densities, leads to mass distributions similar to those found on real bones. Results show that the

proposed remodelling process can account at the same time for both biological and mechanical requirements. In fact, this work shows that the most influential parameter is the bone specific surface, whose dependence on porosity allows controlling both bone composition and, at the same time, to enhance biological functions in areas of low mechanical loading demands that require mineral interchange with the blood. But while the specific surface area controls the density of activated BMUs per unit time, the removal strategy determines the correct tissue composition and, therefore, its mineral distribution. Provided the relation between loads and initial bone density is not too extreme (which would lead to unrealistic damage escalation), proper apparent density distributions, as well as other related parameters (e.g., mineralization level, BMU activity, stress distribution) emerge naturally from the model. As a result, the boomerang-shape relationship between apparent and material densities [28] is fulfilled throughout the bone volume, which suggests that the model is able to capture not only the clear differences between cortical and cancellous zones, but the more subtle ones.

Additionally, when removing the external loads (disuse condition), the model shows a good agreement with the measurement of bone mass loss in astronauts after space flights. Interestingly, the numerical predictions could be used the other way around to determine the best daily physical exercise plans needed to fend off excessive resorption in a personalized manner.

The model presents, however, some limitations. For instance, since it is based on continuous mechanics with isotropic elastic properties and the application of complex loads (such as stair climbing, standing up, sitting down, etc.) is limited, the model is not able yet to account for cancellous bone orientation depending on load direction, microarchitecture, or trabecular thickening. A multiscale, more complex and computationally more expensive approach could be developed to overcome these limitations.

It is worth noting that parameters must be carefully selected (for now, manually) to avoid developing fictitious density distributions. However, this initialization could be driven and automatized by customizing the stimulus by using a protocol that transformed tomographic images into real initial bone geometries (automatic segmentation) with appropriate initial equilibrium stimulus, as proposed in [40]. Hence, the model could be initialized by running a base simulation of the mechanical problem with the reconstructed geometry but deactivating remodelling, computing strain energies without initial damage and imposing the computed stimulus at each point for further simulations. Thus, given an initial configuration practically similar to that of the patient-specific bone, the model would ensure that the distribution of densities will remain under physiological values for normal loads, from which any phenomenon of interest can be studied.

In sum, the model is able, with a proper initialization, to capture a wide range of mechanical and biological variables at the macro-scale (in large 3D geometries) with low computational cost (each simulation takes about 4 days of real time per 8000 days simulated, with a relatively low computational cost), which could be useful as a predictor of bone mass loss or fracture probability in patient-specific therapies, rehabilitation or the consequence of bone-prostheses interaction. Furthermore, the consequences of pathologies such as menopause can be easily implemented by tweaking some of the involved parameters (particularly  $f_{bb}$  and  $f_{bio}$ ) and will be the subject of future studies.

## ACKNOWLEDGEMENTS

Marcelo Berli, Feliciano Franco and José Di Paolo acknowledge Universidad Nacional de Entre Ríos for supporting their work through the PID 6226.

## CONFLICTS OF INTEREST STATEMENT.

The authors of the manuscript entitle “BMU activity linked to mechanical stress, specific surface and inhibitory theory dictate the distribution of mass inside bone. Predictions from a 3D computational model”, certify that they have NO affiliations with or involvement in any organization or entity with any financial interest (such as honoraria; educational grants; participation in speakers’ bureaus; membership, employment, consultancies, stock ownership, or other equity interest; and expert testimony or patent-licensing arrangements), or non-financial interest (such as personal or professional relationships, affiliations, knowledge or beliefs) in the subject matter or materials discussed in this manuscript.

## REFERENCES

- [1] M. Doblaré and J. M. García, “Anisotropic bone remodelling model based on a continuum damage-repair theory,” *J. Biomech.*, vol. 35, no. 1, pp. 1–17, 2002, doi: 10.1016/S0021-9290(01)00178-6.
- [2] E. Seeman, “Bone modeling and remodelling,” *Crit. Rev. Eukaryot. Gene Expr.*, vol. 10, no. 3–4, pp. 219–233, 2000.
- [3] L. J. Raggatt and N. C. Partridge, “Cellular and molecular mechanisms of bone remodelling,” *J. Biol. Chem.*, vol. 285, no. 33, pp. 25103–25108, 2010, doi: 10.1074/jbc.R109.041087.
- [4] US Department of Health and Human Services, “Bone health and osteoporosis: a report of the Surgeon General,” *US Heal. Hum. Serv.*, p. 437, 2004. Available [Online]: <https://www.ncbi.nlm.nih.gov/books/NBK45513/>
- [5] Y. Kameo, Y. Miya, M. Hayashi, T. Nakashima, and T. Adachi, “In silico experiments of bone remodelling explore metabolic diseases and their drug treatment,” *Sci. Adv.*, vol. 6, no. 10, pp. 1–11, 2020, doi: 10.1126/sciadv.aax0938.
- [6] N. Rucci, “Molecular Biology of Bone Biology,” *Clin. Cases Miner. Bone Metab.*, vol. 5, no. 1, pp. 49–56, 2008.
- [7] M. Berli *et al.*, “Localized tissue mineralization regulated by bone remodelling: A computational approach,” *PLoS One*, vol. 12, no. 3, pp. 1–19, 2017, doi: 10.1371/journal.pone.0173228.
- [8] M. Doblaré and J. M. García, “Application of an anisotropic bone-remodelling model based on a damage-repair theory to the analysis of the proximal femur before and after total hip replacement,” *J. Biomech.*, vol. 34, no. 9, pp. 1157–1170, 2001, doi: 10.1016/S0021-9290(01)00069-0.
- [9] R. Huiskes, R. Ruimerman, G. H. van Lenthe, and J. D. Janssen, “Effects of mechanical forces on maintenance and adaptation of form in trabecular bone,” *Nature*, vol. 405, no. 6787, pp. 704–706, Jun. 2000, doi: 10.1038/35015116.

- [10] J. Martínez-Reina, J. M. García-Aznar, J. Domínguez, and M. Doblaré, "On the role of bone damage in calcium homeostasis," *J. Theor. Biol.*, vol. 254, no. 3, pp. 704–712, Oct. 2008, doi: 10.1016/j.jtbi.2008.06.007.
- [11] L. J. Raggatt and N. C. Partridge, "Cellular and Molecular Mechanisms of Bone Remodelling \*," vol. 285, no. 33, pp. 25103–25108, 2010, doi: 10.1074/jbc.R109.041087.
- [12] M. Kutz, *Biomedical Engineering and Design Handbook*. 2011.
- [13] A. M. Parfitt, *Skeletal Heterogeneity and the Purposes of Bone Remodelling: Implications for the Understanding of Osteoporosis*, Fourth Edi. Elsevier, 2013.
- [14] R. Martin, "Toward a unifying theory of bone remodelling," *Bone*, vol. 26, no. 1, pp. 1–6, Jan. 2000, doi: 10.1016/S8756-3282(99)00241-0.
- [15] J. Martínez-Reina, I. Reina, J. Domínguez, and J. M. García-Aznar, "A bone remodelling model including the effect of damage on the steering of BMUs," *J. Mech. Behav. Biomed. Mater.*, vol. 32, pp. 99–112, Apr. 2014, doi: 10.1016/j.jmbbm.2013.12.025.
- [16] R. Huiskes, R. Ruimerman, G. H. van Lenthe, and J. D. Janssen, "Effects of mechanical forces on maintenance and adaptation of form in trabecular bone.," *Nature*, vol. 405, no. 6787, pp. 704–6, Jun. 2000, doi: 10.1038/35015116.
- [17] D. Grimm *et al.*, "The impact of microgravity on bone in humans," *Bone*, vol. 87, pp. 44–56, 2016, doi: 10.1016/j.bone.2015.12.057.
- [18] T. Cervinka, H. Sievänen, J. Hyttinen, and J. Rittweger, "Bone loss patterns in cortical, subcortical, and trabecular compartments during simulated microgravity," *J. Appl. Physiol.*, vol. 117, no. 1, pp. 80–88, 2014, doi: 10.1152/jappphysiol.00021.2014.
- [19] H. C. Blair, "How the osteoclast degrades bone," *BioEssays*, vol. 20, no. 10, pp. 837–846, 1998, doi: 10.1002/(SICI)1521-1878(199810)20:10<837::AID-BIES9>3.0.CO;2-D.
- [20] H. K. Väänänen and H. Zhao, "Osteoclast Function. Biology and Mechanisms.," *Princ. Bone Biol. Two-Volume Set*, vol. 1, pp. 193–209, 2008, doi: 10.1016/B978-0-12-373884-4.00030-6.
- [21] P. Pivonka, P. R. Buenzli, S. Scheiner, C. Hellmich, and C. R. Dunstan, "The influence of bone surface availability in bone remodelling-A mathematical model including coupled geometrical and biomechanical regulations of bone cells," *Eng. Struct.*, vol. 47, pp. 134–147, 2013, doi: 10.1016/j.engstruct.2012.09.006.
- [22] R. B. Martin, "Porosity and specific surface of bone.," *Crit. Rev. Biomed. Eng.*, vol. 10, no. 3, pp. 179–222, 1984.
- [23] Adams G, Cook R, Hutchinson J, Zioupos P, 'Bone surface distribution across a wide porosity range in mammalian bone tissue.' World Congress Biomechanics (WCB) July 6-11, 2014; Boston, MA, USA
- [24] G. Karsenty, "The genetic transformation of bone biology," *Genes Dev.*, vol. 13, no. 23, pp. 3037–3051, 1999, doi: 10.1101/gad.13.23.3037.
- [25] M. A. Hartmann, J. W. C. Dunlop, Y. J. M. Bréchet, P. Fratzl, and R. Weinkamer, "Trabecular bone remodelling simulated by a stochastic exchange of discrete bone

- packets from the surface," *J. Mech. Behav. Biomed. Mater.*, vol. 4, no. 6, pp. 879–887, 2011, doi: 10.1016/j.jmbbm.2011.03.005.
- [26] C. Lukas *et al.*, "Mineralization kinetics in murine trabecular bone quantified by time-lapsed in vivo micro-computed tomography," *Bone*, vol. 56, no. 1, pp. 55–60, 2013, doi: 10.1016/j.bone.2013.05.005.
- [27] E. F. Eriksen, "Cellular mechanisms of bone remodelling", *Rev. Endocr. Metab. Disord.*, vol. 11, no. 4, pp. 219–227, 2010, doi: 10.1007/s11154-010-9153-1.
- [28] P. Zioupos, R. B. Cook, and J. R. Hutchinson, "Some basic relationships between density values in cancellous and cortical bone", *J. Biomech.*, vol. 41, no. 9, pp. 1961–1968, 2008, doi: 10.1016/j.jbiomech.2008.03.025.
- [29] J. M. Reina, J. M. García-Aznar, J. Domínguez, and M. Doblaré, "Numerical estimation of bone density and elastic constants distribution in a human mandible", *J. Biomech.*, vol. 40, no. 4, pp. 828–836, Jan. 2007, doi: 10.1016/j.jbiomech.2006.03.007.
- [30] J. M. García-Aznar, T. Rueberg, and M. Doblare, "A bone remodelling model coupling microdamage growth and repair by 3D BMU-activity", *Biomech. Model. Mechanobiol.*, vol. 4, no. 2–3, pp. 147–167, Nov. 2005, doi: 10.1007/s10237-005-0067-x.
- [31] C. A. Pattin, W. E. Caler, and D. R. Carter, "Cyclic mechanical property degradation during fatigue loading of cortical bone", *J. Biomech.*, vol. 29, no. 1, pp. 69–79, 1996, doi: 10.1016/0021-9290(94)00156-1.
- [32] B. Mikić and D. R. Carter, "Bone strain gage data and theoretical models of functional adaptation", *J. Biomech.*, vol. 28, no. 4, pp. 465–469, Apr. 1995, doi: 10.1016/0021-9290(94)00085-1.
- [33] J. D. Currey, "Tensile yield in compact bone is determined by strain, post-yield behaviour by mineral content", *J. Biomech.*, vol. 37, no. 4, pp. 549–56, Apr. 2004, doi: 10.1016/j.jbiomech.2003.08.008.
- [34] J. Martínez-Reina, J. Ojeda, and J. Mayo, "On the use of bone remodelling models to estimate the density distribution of bones uniqueness of the solution", *PLoS One*, vol. 11, no. 2, pp. 1–17, 2016, doi: 10.1371/journal.pone.0148603.
- [35] M. Heller, G. Bergmann, J. Kassi, L. Claes, N. Haas and Duda G, "Determination of muscle loading at the hip joint for use in pre-clinical testing", *J Biomech.* Vol. 38, pp. 1155-1163, 2005. Doi: 10.1016/j.jbiomech.2004.05.022
- [36] B. Behrens, I. Nolte, P. Wefstaedt, C. Stukenborg-Colsman, and A. Bouguechea, "Numerical investigations on the strain-adaptive bone remodelling in the periprosthetic femur: Influence of the boundary conditions", *Biomed Eng Online*, vol. 8, pp. 1-9, doi: 10.1186/1475-925X-8-7.
- [37] S. Singh and S. P. Singh, "Weight of the femur - a useful measurement for identification of sex", *Acta Anat.*, vol. 87, pp. 141–145, 1974.
- [38] T. M. Maden-Wilkinson, J. S. McPhee, J. Rittweger, D. A. Jones, and H. Degens, "Thigh muscle volume in relation to age, sex and femur volume," *Age*, vol. 36, no. 1, pp. 383–393, 2014, doi: 10.1007/s11357-013-9571-6.
- [39] B. L. Yale., "Yale University Histology Image Gallery."

[http://medcell.med.yale.edu/systems\\_cell\\_biology/bone\\_lab.php](http://medcell.med.yale.edu/systems_cell_biology/bone_lab.php).

[40] M. Berli. PHD thesis. Universidad Nacional de Entre Ríos. Argentina. 2020.